# Nanobody-directed targeting of optogenetic tools reveals differential regulation of cilia length

Jan N. Hansen[1#], Fabian Kaiser[1#], Christina Klausen[1], Birthe Stüven[1], Raymond Chong[1], Wolfgang Bönigk[2], David U. Mick[3], Andreas Möglich[4,5,6], Nathalie Jurisch-Yaksi[7,8], Florian I. Schmidt[9,10]*, Dagmar Wachten[1,11]*

[1] Institute of Innate Immunity, Biophysical Imaging, Medical Faculty, University of Bonn, 53127 Bonn, Germany
[2] Department of Molecular Sensory Systems, Center of Advanced European Studies and Research (caesar), 53175 Bonn, Germany
[3] Center for Molecular Signaling (PZMS), Center of Human and Molecular Biology (ZHMB), Saarland University, School of Medicine, 66421 Homburg, Germany
[4] Lehrstuhl für Biochemie, Universität Bayreuth, 95447 Bayreuth, Germany
[5] Research Center for Bio-Macromolecules, Universität Bayreuth, 95447 Bayreuth, Germany
[6] Bayreuth Center for Biochemistry & Molecular Biology, Universität Bayreuth, 95447 Bayreuth, Germany
[7] Kavli Institute for Systems Neuroscience and Centre for Neural Computation, The Faculty of Medicine, Norwegian University of Science and Technology, Trondheim, Norway
[8] Department of Neurology and Clinical Neurophysiology, St. Olavs University Hospital, Trondheim, Norway
[9] Institute of Innate Immunity, Emmy Noether research group, Medical Faculty, University of Bonn, 53127 Bonn, Germany
[10] Core Facility Nanobodies, University of Bonn, 53127 Bonn, Germany
[11] Research Group Molecular Physiology, Center of Advanced European Studies and Research (caesar), 53175 Bonn, Germany

# equally contributed

* corresponding authors:

Florian I. Schmidt, Institute of Innate Immunity, Emmy Noether research group, Medical Faculty, University of Bonn, 53127 Bonn, Germany. fschmidt@uni-bonn.de, +49-228-28751124

Dagmar Wachten, Institute of Innate Immunity, Biophysical Imaging, Medical Faculty, University of Bonn, 53127 Bonn, Germany, dwachten@uni-bonn.de, +49-228-9656-311, orcid: 0000-0003-4800-6332

**Keywords**

Cilia, optogenetics, nanobodies, cyclic AMP

**Abstract**

Compartmentalization of cellular signaling forms the molecular basis of cellular behavior. Primary cilia constitute a subcellular compartment that orchestrates signal transduction independent from the cell body. Ciliary dysfunction causes severe diseases, termed ciliopathies. Analyzing ciliary signaling and function has been challenging due to the lack of tools to manipulate and analyze ciliary signaling in living cells. Here, we describe a nanobody-based targeting approach for optogenetic tools that allows to specifically analyze ciliary signaling and function, and that is applicable *in vitro* and *in vivo*. We overcome the loss of protein function observed after direct fusion to a ciliary targeting sequence, and functionally localize the photo-activated adenylate cyclase bPAC, the light-activated phosphodiesterase LAPD, and the cAMP biosensor mlCNBD-FRET to the cilium. Using this approach, we unravel the contribution of spatial cAMP signaling in controlling cilia length. Combining optogenetics with nanobody-based targeting will pave the way to the molecular understanding of ciliary function in health and disease.

## Introduction

Primary cilia are membrane-encased protrusions that extend from the surface of almost all vertebrate cells. Primary cilia function as antennae that translate sensory information into a cellular response. The sensory function is governed by a subset of receptors and downstream signaling components that are specifically targeted to the cilium. This allows to orchestrate rapid signal transduction in a minuscule reaction volume, independent of the cell body. A central component of ciliary signaling is the second messenger 3', 5'-cyclic adenosine monophosphate (cAMP) (Johnson & Leroux, 2010). The prime example is chemosensation in highly specialized olfactory cilia: odorant-induced activation of G protein-coupled receptors (GPCRs) stimulates the synthesis of cAMP by the transmembrane adenylate cyclase 3 (AC3). The ensuing increase in ciliary cAMP levels activates cyclic nucleotide-gated ion channels (CNG), resulting in a depolarization that spreads from the cilium to the synapse (Kaupp, 2010). In recent years, it emerged that cAMP also controls signaling in primary cilia. AC3 is highly enriched in primary cilia and widely used as a ciliary marker (Antal, Benardais et al., 2017, Bishop, Berbari et al., 2007). Loss-of-function mutations in the *ADCY3* gene, encoding for AC3, or loss of *ADCY3* expression cause monogenic severe obesity and increase the risk for type 2 diabetes (Cao, Chen et al., 2016, Grarup, Moltke et al., 2018, Nordman, Ding et al., 2005, Saeed, Bonnefond et al., 2018, Siljee, Wang et al., 2018, Wang, Li et al., 2009). This has been attributed to the loss of AC3 function in neuronal primary cilia (Barroso, 2018, Siljee et al., 2018). Furthermore, the most prominent primary cilia signaling pathway, the Sonic hedgehog (Shh) pathway, utilizes cAMP as a second messenger in the cilium to transduce stimulation by Shh into a change in gene expression (Moore, Stepanchick et al., 2016, Mukhopadhyay, Wen et al., 2013). Finally, the dynamic modulation of primary cilia length seems to be controlled by cAMP (Besschetnova, Kolpakova-Hart et al., 2010, Porpora, Sauchella et al., 2018). However, as of yet, it has been impossible to manipulate cAMP dynamics in primary cilia independently from the cell body. Hence, the composition and dynamics of cAMP-signaling pathways in primary cilia remain largely unknown.

Optogenetics might be the key to overcome this issue, not least because it has already proven as a powerful method to manipulate and monitor cAMP dynamics in mouse sperm flagella, a specialized motile cilium (Balbach, Beckert et al., 2018, Jansen, Alvarez et al., 2015, Mukherjee, Jansen et al., 2016). The photo-activated adenylate cyclase bPAC (Stierl, Stumpf et al., 2011) has been employed to increase flagellar cAMP levels by blue light (Jansen et al., 2015), and the FRET-based cAMP biosensor mlCNBD-FRET has been used to monitor cAMP dynamics in sperm flagella (Mukherjee et al., 2016). This cAMP tool kit can be complemented with the red light-activated phosphodiesterase LAPD that allows to decrease cAMP levels in a light-dependent manner (Gasser, Taiber et al., 2014, Stabel, Stüven et al., 2019). In cells other

than sperm, the challenge is to specifically target these tools to the primary cilium to investigate cAMP signaling in the cilium, but not in the cell body. Free diffusion of proteins into the primary cilium is limited by the transition zone (TZ) at the base of the cilium (Reiter, Blacque et al., 2012). Protein transport into and out of the cilium is controlled by the intraflagellar transport (IFT) machinery in combination with the BBSome, a multi-protein complex at the ciliary base (Berbari, Lewis et al., 2008, Loktev & Jackson, 2013, Nachury, 2018, Rosenbaum & Witman, 2002). The combined action of IFT, BBSome, and TZ shape the unique ciliary protein composition (Nachury & Mick, 2019). To localize a given optogenetic tool to the primary cilium, the ciliary transport machinery needs to be hijacked. Common strategies involve direct fusion to the C terminus of either a full-length GPCR, e.g. the somatostatin receptor 3 (SSTR3) (Berbari et al., 2008), or a truncated ciliary protein, e.g. the first 200 amino acids of the ciliary mouse Nphp3 (nephrocystin 3) protein (Mick, Rodrigues et al., 2015, Wright, Baye et al., 2011). However, the first approach suffers from the limitation that it alters the ciliary set of signal receptors. Here, we show that the latter approach largely failed for LAPD and mlCNBD-FRET, because N-terminal fusion disrupts their optogenetic and biosensoric function, respectively. Therefore, we developed a new technique to hijack the ciliary targeting machine using intracellular nanobodies. The nanobody-based approach allows to specifically target proteins to the primary cilium without directly fusing them to a ciliary protein. Instead, the nanobody is cilia-targeted and tows the proteins of interest to the cilium by binding to a tag contained in the protein of interest.

We show that the cilia-targeted nanobodies bind to eGFP or mCherry fusions of a protein of interest, including bPAC, LAPD, or mlCNBD-FRET, in the cytosol, followed by translocation of the complex into the primary cilium. Nanobody binding does not substantially impair protein function, i.e. light-dependent activation of bPAC and LAPD or cAMP-induced conformational changes of mlCNBD-FRET. We demonstrate the validity of this novel approach both *in vitro* and *in vivo* in mammalian cells and zebrafish, respectively. Moreover, using nanobody-based ciliary targeting of bPAC, we reveal the role of ciliary versus cytosolic (cell body) cAMP signaling in controlling cilia length. Our approach principally extends to the ciliary targeting of any protein of interest, which is recognized by a nanobody. Thereby, the huge variety of genetically-encoded tools to manipulate cellular signaling, e.g. membrane potential, protein-protein interactions, or enzymatic activities, and to monitor cellular signaling, e.g. dynamics of $Ca^{2+}$, pH, or the membrane potential, could be exclusively targeted to the primary cilium using our nanobody-based targeting approach. This strategy opens up new avenues for cilia biology and allows to finally address long-standing questions in cell biology.

## Results

### N-terminal fusion of optogenetic tools interferes with photoactivation

To utilize the optogenetic tools bPAC- or LAPD-mCherry in a cilium-specific manner, we first tested whether N-terminal fusion of mNphp3(201) is sufficient for targeting to the primary cilium. Indeed, fusions of both bPAC and LAPD predominantly localized to the primary cilium (Fig. 1A, B). To test whether protein fusion interferes with the light-dependent activation of LAPD or bPAC, we measured LAPD or bPAC activity using $Ca^{2+}$ imaging. To this end, we used HEK293 cells stably expressing a cyclic nucleotide-gated (CNG) ion channel CNGA2-TM (HEK-TM) that conducts $Ca^{2+}$ upon cAMP binding (Wachten, Schlenstedt et al., 2006). Activation of bPAC with a 465 nm light pulse increases intracellular cAMP levels, leading to a $Ca^{2+}$ influx, which is quantified using the fluorescence of a $Ca^{2+}$ indicator dye (Fig. 1C). To measure LAPD activity, HEK-TM cells were pre-stimulated with NKH477, a water-soluble forskolin analog that activates transmembrane adenylate cyclases (tmACs) and, thereby, increases cAMP levels, leading to a $Ca^{2+}$ influx. NKH477 stimulation was performed under illumination with 850 nm that deactivates LAPD. When the $Ca^{2+}$ influx reached a steady-state, LAPD was activated by 690 nm light, decreasing cAMP levels and, thereby, the intracellular $Ca^{2+}$ concentration (Fig. 1C). We measured the cytosolic mNphp3(201)-bPAC-mCherry or mNphp3(201)-LAPD-mCherry activity and compared its activity to the non-ciliary tagged bPAC- or LAPD-mCherry proteins. Light stimulation of mNphp3(201)-bPAC-mCherry or bPAC-mCherry expressing HEK-TM cells resulted in a transient $Ca^{2+}$ increase, which was absent in mCherry-expressing control cells (Fig. 1D). Repetitive light-stimulation with different light pulses reliably increased the intracellular $Ca^{2+}$ concentration in mNphp3(201)-bPAC-mCherry or bPAC-mCherry expressing HEK-TM cells (Fig. 1D). Normalized peak amplitudes of the $Ca^{2+}$ signal evoked after the first light pulse were lower in HEK-TM cells expressing mNphp3(201)-bPAC-mCherry than in HEK-TM cells expressing bPAC-mCherry (Fig. 1E), indicating that the N-terminal fusion to a ciliary targeting sequence interferes with the light-dependent activation of bPAC. Next, responses of HEK-TM cells stably expressing mNphp3(201)-LAPD-mCherry or LAPD-mCherry to NKH477 stimulation were quantified: in both, mNphp3(201)-LAPD-mCherry and LAPD-mCherry expressing HEK-TM cells, the $Ca^{2+}$ increase after NKH477 stimulation was significantly reduced compared to HEK-TM mCherry cells, indicating that LAPD displays some basal activity even at 850 nm light deactivation (Fig. 1F). Comparing the decrease in the intracellular $Ca^{2+}$ concentration at 690 nm light stimulation, LAPD-mCherry showed a much higher light-dependent activity than mNphp3(201)-LAPD-mCherry (Fig.1 G), indicating that N-terminal fusion to a ciliary targeting sequence also interferes with the light-dependent activation of LAPD. Taken together, our results obtained with two different optogenetic tools revealed that fusion with a ciliary targeting motif interfered with their light-dependent activation, thus hampering a direct targeting strategy.

### Targeting optogenetic tools to the primary cilium using nanobodies

We next devised a combinatorial strategy that allows targeting to the primary cilium, while entirely avoiding N-terminal fusion. Rather, we fused our optogenetic tools with a fluorescent reporter (e.g. mCherry) at their C termini, which leaves photoactivation unaffected (Jansen et al., 2015). To direct these proteins to primary cilia, we co-expressed a nanobody, which is directed against the tag (mCherry) and is fused to the ciliary targeting sequence mNphp3(201) at its N terminus. We hypothesize that the nanobody binds to its target in the cytoplasm, the nanobody-protein-complex is recognized by the IFT machinery, and is then transported into the primary cilium (Fig. 2A). We first tested the anti-mCherry nanobody $VHH_{LaM-2}$ (Ariotti, Rae et al., 2018, Fridy, Li et al., 2014), fused to eGFP at the C terminus and mNphp3(201) at the N terminus, in mIMCD-3 cells. Indeed, the nanobody localized to primary cilia (Fig. 2B). Next, we assessed whether nanobody binding was sufficient to traffic our optogenetic tools to the cilium. Co-expression of the nanobody with LAPD-mCherry resulted in ciliary localization of both the nanobody fusion and LAPD-mCherry (Fig. 2C). In contrast, LAPD-mCherry remained exclusively cytosolic in the absence of the nanobody (Fig. 2D). A second nanobody directed against mCherry, $VHH_{LaM-4}$, (Ariotti et al., 2018, Fridy et al., 2014) also localized to primary cilia and resulted in ciliary localization of LAPD (Sup. Fig. 1A, B), while a nanobody directed against eGFP (Kirchhofer, Helma et al., 2010) did not mediate ciliary localization of LAPD-mCherry (Sup. Fig. 1C). The nanobody-based targeting approach also succeeded in localizing bPAC-mCherry to the primary cilium (Fig. 2E). Taken together, nanobody-based targeting proved efficient and specific. Hence, we assume that our approach is generally applicable to target proteins of interest to cilia.

### Nanobody binding does not interfere with protein function

To test whether nanobody binding interferes with the light-dependent activation of LAPD or bPAC, we measured their activity in HEK-TM cells in the presence or absence of the cilia-targeted mCherry nanobody mNphp3(201)-$VHH_{LaM-2}$-eGFP. Without co-expression of the nanobody, bPAC- and LAPD-mCherry displayed a cytosolic distribution (Fig. 3A, B). In the absence of primary cilia, the cilia-targeted mNphp3(201)-$VHH_{LaM-2}$-eGFP nanobody formed clusters (Fig. 3C), while the $VHH_{LaM-2}$-eGFP nanobody did not (Fig. 3D). Co-expression of bPAC- or LAPD-mCherry with the cilia-targeted nanobody resulted in cluster localization of either bPAC or LAPD, demonstrating that the nanobody interacts with the mCherry fusion-proteins in the cytoplasm (Fig. 3E, F). To verify whether in the absence of cilia, protein clusters formed at centrosomes, HEK293 cells expressing mNphp3(201)-$VHH_{LaM-2}$-eGFP were labeled with a pericentrin antibody (Sup. Fig. 1D). Protein cluster formation did not predominantly occur at centrosomal regions: 52% of the cells showed mNphp3(201)-$VHH_{LaM-2}$-eGFP localization inside the centrosomal region, whereas 48% of the cells displayed localization of the nanobody

outside the centrosomal region (Sup. Fig. 1D, E). To test bPAC or LAPD function in the presence of the nanobody, we compared the light-dependent activation of bPAC or LAPD in the presence or absence of the cilia-targeted mCherry nanobodies $VHH_{LaM-2}$ and $VHH_{LaM-4}$ (fused to either eGFP or a hemagglutinin HA-tag, respectively) or a ciliary protein that does not interact with either bPAC- or LAPD-mCherry (Sstr3-eGFP). Under each condition, photoactivation of bPAC or LAPD activity was retained, demonstrating that the presence of the nanobody does not interfere with protein function (Fig. 3G, H). Of note, light-induced changes of the intracellular cAMP concentration in the cell body can also be directly visualized using a spectrally orthogonal system that includes bPAC-eGFP and the cAMP biosensor R-FlincA (Ohta, Furuta et al., 2018). Photoactivation of bPAC-eGFP in HEK293 cells transiently increased the R-FlincA fluorescence, whereas a non-binding mutant sensor did not respond to bPAC photoactivation (Sup. Fig. 2A, B). In summary, our nanobody-based approach provides a versatile means for ciliary targeting without interfering with protein function.

**Targeting of a genetically-encoded biosensor to the primary cilium**

We previously engineered and applied a genetically-encoded biosensor, named mlCNBD-FRET, to measure cAMP dynamics in motile cilia (Mukherjee et al., 2016). We already demonstrated targeting of this sensor to primary cilia by fusing it to the C terminus of Sstr3 (Mukherjee et al., 2016). However, Sstr3 is a functional GPCR, which may interfere with ciliary signaling upon overexpression. Thus, we first tested whether fusing mNphp3(201) to the N terminus of mlCNBD-FRET also promotes ciliary localization and retains biosensor function. While the biosensor localized to the primary cilium (Fig. 4A), biosensor function was severely impaired as mlCNBD-FRET no longer responded to changes in cAMP levels (Fig. 4B, C). We thus tested whether the biosensor can be targeted to primary cilia using our nanobody-based approach without interfering with protein function. The mlCNBD-FRET sensor consists of the FRET pair cerulean and citrine (Mukherjee et al., 2016). Both fluorescent proteins are recognized by the nanobody $VHH_{enhancer}$ directed against eGFP (Kirchhofer et al., 2010, Kubala, Kovtun et al., 2010). Fusion of mNphp3(201) to the N terminus of the anti-eGFP nanobody also resulted in ciliary localization (Fig. 4D). In the absence of the nanobody, mlCNBD-FRET was uniformly distributed throughout the cytosol, whereas co-expression with the cilia-targeted nanobody resulted in ciliary localization of mlCNBD-FRET (Fig. 4E, F). To test whether nanobody interaction impaired mlCNBD-FRET function, we performed FRET imaging in HEK293 cells expressing mlCNBD-FRET in the presence or absence of the nanobody. Similar to the anti-mCherry nanobody, the cilia-targeted eGFP mNphp3(201)-$VHH_{enhancer}$-mCherry nanobody showed a more clustered subcellular localization in HEK293 cells in the absence of primary cilia formation (Fig. 4G). Consistently, when binding to the nanobody, mlCNBD-FRET also formed clusters within the cytosol (Fig. 4H), which did not occur in the presence of mCherry only (Fig. 4I). To functionally test the FRET sensor in the

presence of the nanobody, we first assessed the impact of the nanobody on the fluorescence intensity of the two fluorophores, cerulean and citrine. HEK293 cells were transfected with cerulean or citrine and the eGFP $VHH_{enhancer}$-mCherry nanobody or mCherry only. The fluorescence intensity of cerulean or citrine was normalized to the mCherry fluorescence in the same cell. Both cerulean and citrine showed an increase in fluorescence in the presence of the nanobody compared to the mCherry control as previously described (Kirchhofer et al., 2010), but the relative change for each of the fluorophores was not substantially different (Sup. Fig. 3). To test whether mICNBD-FRET:nanobody complexes still respond to changes in cAMP levels, we measured changes in FRET after addition of 20 μM isoproterenol, which stimulates AC activity through signaling via GPCRs (G protein-coupled receptors). To this end, we tested both, the FRET response in HEK293 mICNBD-FRET co-expressing the ciliary-tagged eGFP nanobody mNphp3(201)-$VHH_{enhancer}$-mCherry or the non-targeted $VHH_{enhancer}$-mCherry nanobody. In the presence of the non-targeted nanobody, the FRET response to stimulation with isoproterenol remained unchanged (Fig. 4J, K). Interaction with the cilia-targeted nanobody only marginally reduced the FRET response and generally left the reporter functional (Fig. 4J, K). In contrast, the mNphp3(201)-mICNBD-FRET fusion did not respond to changes in cAMP at all (Fig. 4B). The expression level of the mNphp3(201)-mICNBD-FRET fusion and mICNBD-FRET, determined by their absolute fluorescence intensities, were not different: mICNBD-FRET: cerulean: 207 ± 4 a.u., citrine: 899 ± 46 a.u.; mNPHP3(201)-mICNBD-FRET: cerulean: 212 ± 10 a.u., citrine: 923 ± 86 a.u.., allowing a direct comparison. Lastly, we performed FRET imaging in cilia of mIMCD-3 cells expressing mICNBD-FRET and mNphp3(201)-$VHH_{enhancer}$-mCherry and measured the response to stimulation with 250 μM IBMX, a broad-band phosphodiesterase inhibitor. The ciliary-localized mICNBD-FRET responded with a change in FRET upon stimulation (Fig. 4L). In summary, the nanobody-based approach also can be used to target genetically-encoded biosensors to the primary cilium.

**Applying the nanobody-based ciliary targeting approach *in vivo***

Having shown that our bipartite strategy for localization to primary cilia works *in vitro*, we wondered whether we could also target proteins of interest to primary cilia *in vivo*. We first confirmed the ciliary localization of the nanobody *in vivo* by injecting mRNA of the anti-mCherry mNphp3(201)-$VHH_{LaM-2}$-eGFP nanobody into nacre *(mitfa$^{-/-}$)* zebrafish embryos, which are transparent and, therefore, widely used for fluorescence imaging (Lister, Robertson et al., 1999). The cilia-targeted nanobody was expressed and localized to cilia in all tissues, including the developing neural tube, the primary and motile cilia of the spinal cord (Kramer-Zucker, Olale et al., 2005), and the eye (Fig. 5A, B, C) and allowed to mark cilia in an *in vivo* imaging approach (Supp. Fig. 3A). Localization of the nanobody to cilia is similar to the previously

described *bactin:arl13b-gfp* transgenic line, where GFP is fused to the ciliary Arl13B protein (Supp. Fig. 4) (Borovina, Superina et al., 2010, Olstad, Ringers et al., 2019). To test whether the cilia-targeted nanobody can also direct proteins to primary cilia *in vivo*, we injected mRNA of the anti-mCherry nanobody fusion mNphp3(201)-$VHH_{LaM-2}$-eGFP into transgenic zebrafish embryos ubiquitously expressing RFP (*Ubi:zebrabow*) (Pan, Freundlich et al., 2013), which is also bound by the anti-mCherry nanobody. In the absence of the nanobody, RFP was distributed in the cytosol (Fig. 5D, Supp. Fig. 4C). In the presence of the nanobody, RFP was highly enriched in primary cilia (Fig. 5E, Supp. Fig. 4D), demonstrating that our nanobody-based approach efficiently targets ectopically expressed proteins to primary cilia and to motile cilia *in vitro* and *in vivo*.

**Investigating the spatial contribution of cAMP signaling to cilia length control**

The primary cilium is a dynamic cellular structure that assembles and dissembles in accordance with the cell cycle (Keeling, Tsiokas et al., 2016, Kim & Tsiokas, 2011, Wang, Ren et al., 2019). The interplay between assembly and disassembly determines the length of the primary cilium. cAMP-dependent signaling pathways have been shown to regulate cilia length (Avasthi, Marley et al., 2012, Besschetnova et al., 2010, Kwon, Temiyasathit et al., 2010, Porpora et al., 2018). However, it has been controversially discussed whether an increase in the intracellular cAMP concentration, evoked by pharmacological stimulation, results in an increase or decrease in cilia length (Besschetnova et al., 2010, Porpora et al., 2018). In fact, we also performed pharmacological stimulation of cAMP synthesis in mIMCD-3 cells using forskolin and analyzed the change in cilia length. However, our data was quite variable and we did not observe a significant change in cilia length (Fig. 6A). Pharmacological stimulation of cAMP synthesis occurs in the whole cell without any spatial confinement. However, cAMP signaling generally occurs within defined subcellular cAMP compartments to evoke a specific cellular response (Johnstone, Agarwal et al., 2018). Whether cAMP synthesis and downstream signaling occurs in the cilium or through interaction with the cell body to control the length of primary cilia, is not known. Thus, we set out to investigate whether an increase in cAMP levels in the cilium using nanobody-based targeting in combination with optogenetics is sufficient to change cilia length.

To this end, we used the monoclonal IMCD-3 cell line stably expressing bPAC-mCherry in combination with the cilia-targeted mNphp3(201)-$VHH_{LAM-2}$-EGFP nanobody. Since ectopic expression of a ciliary protein may result in an increase of the cilia length (Guadiana, Semple-Rowland et al., 2013), we first tested whether expression of the ciliary-tagged nanobody had an impact on the length of the cilium. Indeed, ectopic expression of the nanobody resulted in longer cilia compared to non-transfected control cells. There was a linear correlation between the expression level of the nanobody in the cilium and the cilia length: the higher the expression

(determined by eGFP fluorescence), the longer the cilia (Fig. 6B). However, in the low expression regime, i.e. < 7.5 a.u. eGFP fluorescence, there was no correlation between the expression level and the cilia length (Fig. 6B inset, Fig. 6C). Thus, the amount of protein in the cilium has to be carefully titrated and a thorough analysis is needed to rule out any unspecific effects caused by ectopic expression of the protein. In the following, we hence only analyzed cilia with an expression level of < 7.5 a.u. GFP. We compared the change in cilia length upon photoactivation of bPAC-mCherry either in the cell body or in the presence of mNphp3(201)-$VHH_{LaM-2}$-eGFP in the cilium (Fig. 6D-G). Stimulating cAMP synthesis by light in the cell body significantly reduced cilia length (Fig. 6E, G), whereas stimulating cAMP synthesis in the cilium significantly increased cilia length (Fig. 6F, G).

Next, we complemented our analysis by investigating whether reducing cAMP levels in either the cell body or the cilium using photoactivation of LAPD also changed cilia length. We compared the change in cilia length upon photoactivation of LAPD-mCherry either in the cell body or in the presence of mNphp3(201)-VHHLaM-2-eGFP in the cilium. However, stimulation of LAPD activity neither in the cell body, nor in the cilium, had an effect on cilia length (Fig. 6H-J). We verified whether photoactivation of LAPD in the cell body reduced basal cAMP levels and in fact, total cAMP levels where slightly, but significantly reduced (Sup. Fig. 5D). The changes, however, are much smaller than the dramatic increase in cAMP levels observed after photoactivation of bPAC (Sup. Fig. 5A). The cAMP-dependent signaling pathways that control the length of the cilium seem to be sensitive to an increase, but not to a decrease of the basal cAMP concentration. In summary, cAMP-dependent signaling pathways in the cell body or the cilium evoke opposing effects on cilia length control, demonstrating how compartmentalized cAMP signaling determines specific ciliary and, thereby, cellular functions.

## Discussion

The primary cilium constitutes a unique subcellular compartment. However, our understanding of how specific ciliary signaling pathways control cellular functions is still limited. Optogenetics is an apt method to measure and manipulate ciliary signaling independent of the rest of the cell. Yet, the use of optogenetic tools in cilia research has been hampered by the fact that some of the tools do not tolerate fusion with a targeting sequence, in particular at the N terminus. We have therefore developed a nanobody-based approach to target optogenetic tools or genetically-encoded biosensors to primary cilia *in vitro* and *in vivo*, while preserving protein function. This novel strategy principally extends to other proteins of interest and subcellular domains. The only requirement is fusion of the protein of interest to a tag or partner that is recognized by the nanobody, without impairing protein function. This is combined with fusion of the nanobody to a targeting sequence for the specific subcellular compartment. This approach is particularly useful for proteins, the function of which is impaired by fusion to a targeting sequence, as we have shown here for the light-activated phosphodiesterase LAPD and the mICNBD-FRET sensor.

Optogenetic tools have been used in motile cilia, i.e. sperm flagella (Balbach et al., 2018, Jansen et al., 2015), where no specific targeting sequence is needed. When expressed under the control of the sperm-specific protamine-1 promoter, bPAC exclusively localized to sperm flagella and allowed to control sperm signaling and function by light (Jansen et al., 2015). However, this approach does not work for primary cilia. Genetically-encoded biosensors for cAMP and $Ca^{2+}$ have already been targeted to primary cilia (Delling, DeCaen et al., 2013, Delling, Indzhykulian et al., 2016, Jiang, Falcone et al., 2019, Moore et al., 2016, Mukherjee et al., 2016). These sensors have been fused to the C terminus of full-length GPCRs, e.g. 5-HT6 (5-hydroxytryptamine receptor 6) (Moore et al., 2016). Yet, overexpression of GPCRs like 5-HT6 causes abnormal cilia growth (Guadiana et al., 2013), limiting this targeting approach. Our results demonstrate that a high expression level of the nanobody in the cilium is also sufficient to increase cilia length (Fig. 6B). Thus, the amount of protein in the cilium has to be carefully titrated and a thorough analysis, like we present here, is needed to rule out any unspecific effects caused by overexpression of the protein.

Targeting proteins to a specific location using nanobodies has been applied to study protein-protein interaction in cells (Herce, Deng et al., 2013) and *Drosophila* (Harmansa, Alborelli et al., 2017). Herce et al. fused an anti-GFP nanobody to the lac repressor to localize the nanobody and its GFP-fused interaction partner to the nucleus. Using this approach, the authors have studied binding and disruption of p53 and HDM2 (human double minute 2), one of the most important protein interactions in cancer research (Herce et al., 2013). Harmansa et al. have mislocalized transmembrane proteins, cytosolic proteins, and morphogens in

*Drosophila* to study the role of correct protein localization for development *in vivo* (Harmansa et al., 2017). Targeting to organelles using nanobodies has also been achieved for two specific proteins, p53 and survivin (Beghein, Van Audenhove et al., 2016, Steels, Verhelle et al., 2018). For primary cilia, nanobodies have been used to investigate the ciliary diffusion barrier (Breslow, Koslover et al., 2013). Here, proteins fused to anti-GFP nanobodies have been recombinantly expressed and added to semi-intact cells expressing cilia-localized GFP. By assessing the ability to capture nanobody-fused proteins of different sizes within cilia, a size cutoff for free diffusion across the ciliary barrier of around 100 kDa was determined (Kee, Dishinger et al., 2012). Although larger proteins can enter cilia by active transport processes, this size cutoff may limit the size of proteins that can be targeted to cilia by a piggyback mechanism using a cilia-localized nanobody. Importantly, a recently developed nanobody, targeting a small alpha-helical epitope tag of 13 amino acids, NbALFA, also works in the cytosol and may reduce the overall size of the protein complexes targeted to primary cilia (Götzke, Kilisch et al., 2019).

Since several signaling (and other) proteins proposed to function in cilia also have well-known functions outside the cilium (such as PKA or AMPK), it is a major challenge in cilia biology to specifically interfere with their cilium-specific functions. One approach is to target proteins or peptides with inhibitory functions specifically to the cilium, e.g. to interfere with PKA activity inside cilia (Mick et al., 2015). Cilia length is an important parameter that determines cilia function (Hsu, Chuang et al., 2017). However, the spatial contribution of signaling pathways in the cilium or cell body that regulate cilia length is not well understood. Using our approach to optogenetically manipulate cAMP levels in the cilium or cell body allows to address the spatial contribution of cAMP signaling in cilia length control. However, the use of optogenetic tools can be challenging due to their residual activity in the dark. In fact, bPAC also displays residual dark activity, whereby cAMP levels in the cell were slightly increased, even without light stimulation (Sup. Fig. 5A). In turn, the change in cAMP level in the cell body already reduced cilia length, even in the dark (Sup. Fig. 5B). We tested different conditions to optimize our protocol, i.e. we analyzed cilia length at different time points (48 h instead of 24 h serum-starvation). The cilia length in mIMCD-3 control cells was similar between the two time points, but the effect of bPAC dark activity on cilia length was significantly reduced after 48 h compared to 24 h (Sup. Fig. 5B, C). Thus, we used this protocol for manipulating cAMP levels in the cell body. One possible explanation why a longer starvation time is beneficial might be that cAMP levels are already important during ciliogenesis. Thus, increased cAMP levels in the cell body due to bPAC dark activity might negatively influence ciliogenesis and only the prolonged time for cilia formation allows to overcome this.

Our results indicate that an increase in cAMP levels and, thereby, cAMP signaling in the cilium or the cell body exert opposing effects by either increasing or decreasing cilia length,

respectively (Fig. 6L). Indeed, it has been demonstrated in HEK293 cells that an increase in cellular cAMP levels and concomitant PKA-dependent protein phosphorylation at centriolar satellites induces ubiquitination and proteolysis of NEK10 by the co-assembled E3 ligase CHIP and promotes cilia resorption (Porpora et al., 2018). This is supported by elegant studies of cilia length control in *Chlamydomonas* (Cao, Meng et al., 2013, Hendel, Thomson et al., 2018, Hu, Liang et al., 2015, Ishikawa & Marshall, 2017, Liang, Zhu et al., 2018, Ludington, Ishikawa et al., 2015, Luo, Cao et al., 2011, Meng & Pan, 2016, Pan & Snell, 2005, Wang et al., 2019). Here, the IFT machinery and its regulation by phosphorylation plays an important role. There is a negative correlation between IFT particles entering flagella and flagella length, suggesting a length-dependent feedback control of IFT entry and, thereby, flagella length. At least in *Chlamydomonas*, phosphorylation of the kinesin-II subunit Fla8 (pFla8) by the calcium-dependent kinase 1 (CDPK1), a homolog of CAMKII, changes the rate of IFT entry and, thereby, flagella length (Liang et al., 2018). Thus, a cellular sensing system controls pFla8 levels, reduces the rate of IFT entry and controls flagella length. In contrast, stimulation of cAMP signaling in the cilium results in an increase in cilia length, probably through cAMP/PKA-dependent signaling pathways, as suggested by experiments in primary cilia of epithelia and mesenchymal cells, where cilia elongation is induced by a cAMP/PKA-dependent mechanism (Besschetnova et al., 2010). Future experiments need to reveal the detailed molecular mechanisms underlying the spatial regulation of length control in mammalian primary cilia.

Our approach and complementary developments in other labs (Beghein et al., 2016, Harmansa et al., 2017, Herce et al., 2013, Steels et al., 2018) open up new avenues for analyzing signaling pathways in primary and motile cilia, as demonstrated by the application of the cilia-targeted nanobody in zebrafish, and beyond that in many other subcellular domains *in vitro* and *in vivo*. The nanobody-based targeting approach conveys high specificity through a strong interaction with its binding partner ($K_d$ ~ 1 nM), which is a prerequisite for subcellular targeting and binding of endogenously expressed proteins *in vitro* and *in vivo* (Beghein & Gettemans, 2017, Van Overbeke, Wongsantichon et al., 2015). In addition, nanobodies are small (~ 15 kDa) and genetically-encoded on one single open reading frame (Beghein & Gettemans, 2017). Thus, the generation of transgenic animals, e.g. mice or zebrafish, expressing the nanobody targeted to a subcellular compartment is straightforward. Analogous to the Cre/loxP recombinase system, the nanobody-based targeting approach offers endless combinations of targeting any protein of interest to a desired subcellular compartment by simply crossing different transgenic lines. This will greatly facilitate the analysis of cellular signaling in the whole cell and in a specific compartment *in vivo*. Conditional expression patterns will further allow temporally controlled recruitment or cell-type specific localization. Many transgenic animals have already been generated, expressing optogenetic tools that are either fused to a fluorescent protein or even contain fluorescent proteins as functional read-

out, e.g. biosensors for second messengers. Combining these transgenic lines with transgenic animals that allow nanobody-based subcellular targeting will pave the way for a more systematic and nuanced application of optogenetics to study cellular signaling. Such studies will unravel how subcellular compartments control cellular functions under physiological and pathological conditions.

## Material and methods

### Plasmids

Coding sequences for codon-optimized anti-mCherry nanobodies $VHH_{LaM-2}$ and $VHH_{LaM-4}$ were synthesized as GeneBlocks by IDT, based on the amino acid sequences provided by Fridy et al., 2018. A vector encoding the anti-eGFP nanobody GBP-1 ($VHH_{Enhancer}$) (Kirchhofer et al., 2010) was kindly provided by the lab of Hidde Ploegh (Boston Children's Hospital, Boston, MA, USA). Information regarding the cloning can be found in the SI Appendix and in Supplementary Table 1.

### Cell lines and tissue culture

HEK293 (CRL-1573) and mIMCD-3 (CRL-2123) cells were obtained from American Type Culture Collection (ATCC). HEK293 TM (HEK-TM) cells were generated as described previously (Wachten et al., 2006). HEK-TM cells were transfected with pc3.1-bPAC-mCherry or pcDNA6-LAPD-mCherry and selected for stable expression. HEK-mICNBD-FRET were generated as described previously (Mukherjee et al., 2016). Information regarding the cultivation of the cell lines can be found in the SI Appendix.

### Transfection

mIMCD-3 cellls were transfected with Lipofectamine 2000 (Thermo Fisher Scientific) and HEK293 cells with polyethylenimine (PEI, Sigma Aldrich). Details are described in the SI Appendix. All cells referred to as non-transfected (NT) were subjected to the same transfection protocol as transfected cells, but without adding DNA, Lipofectamine and PEI.

### Immunocytochemistry

Immunocytochemistry was performed according to standard protocols. Detailed information can be found in the SI Appendix.

### Optogenetic stimulation for cilia length measurements

mIMCD-3 cells and mIMCD-3 bPAC cells were seeded, transfected with pcDNA3.1-mNphp3(201)-$VHH_{LaM-2}$-eGFP, and induced to form cilia as described above. Cells were kept in the dark during the entire experiment and handled only under dim red (bPAC) or green (LAPD) light, preventing bPAC- or LAPD-activation, respectively. For "light" stimulation, cells were placed on a LED plate (bPAC: 465 nm, 38.8 µW/cm²; LAPD: 630 nm, 42.3 µW/cm²) for the last 16 h before harvesting or for 1 h at 24 h prior to harvesting (as indicated in the figure legends). Cells were fixed and further analyzed by immunocytochemistry and confocal microscopy.

### Confocal microscopy and image analysis

Confocal z-stacks (step size 0.4-0.5 µm, 60x objective) were recorded with a confocal microscope (Eclipse Ti, Nikon or Olympus FV100). All depicted images show a maximum projection of a z-stack unless differently stated in the figure legend. Information regarding image analysis can be found in the SI Appendix.

**$Ca^{2+}$ imaging**

$Ca^{2+}$ imaging in 96-well plates in a fluorescence plate reader was performed as previously described (Jansen et al., 2015, Stabel et al., 2019). A detailed protocol and all changes are described in the SI Appendix.

**FRET imaging**

FRET imaging was performed as previously described (Mukherjee et al., 2016). A detailed protocol and all changes are described in the SI Appendix.

**R-FlincA imaging**

HEK293 cells were seeded and transfected with pcDNA4HMB_R-FlincA or pcDNA4HMB_R-FlincAmut (R221E, R335E) (Ohta et al., 2018) (generously provided by Kazuki Horikawa, Tokushima University, Japan) and pEGFP-N1-bPAC (see Supp. Table 1) as described for LAPD activity measurements. Imaging was performed using the CellR Imaging System (Olympus). The experimental recordings were as follows: R-FlincA signal (57% light intensity, 200 ms exposure time, 572/25 excitation filter, mCherry-B-0MF Semrock dichroic mirror, 630/20 emission filter) was measured every 5 s. At 120 s, cells were illuminated for 5 s with 2.1 $mW/cm^2$ white light, followed by further recording of R-FlincA signal every 5 s for 480 s. Subsequently, bPAC-GFP fluorescence (12 % light intensity, 100 ms exposure time, 500/20 excitation filter, M2CFPYFP dichroic mirror, 535-30 emission filter) was measured. Data were analyzed using Fiji/ImageJ (ImageJ Version 1.52i) by selecting low-expressing bPAC-GFP cells with freehand ROIs and determining the mean fluorescence intensity for each ROI in the average signal recorded during the 120 s before white light exposure. Data were plotted as a change of fluorescence over time. Data were acquired from n = 3 measurements.

**Imaging of primary cilia**

mIMCD-3 cells were seeded on PLL (0.1 mg/ml, Sigma Aldrich)-coated chambers (µ-Slide 8 Well Glass Bottom, ibidi) and transfected after 24 h with pc3.1-$VHH_{enhancer}$-HA and pc3.1-mICNBD-FRET (Mukherjee et al., 2016) as described above. The medium was replaced with starvation medium (0.5 % FCS) on the following day to induce ciliogenesis. Confocal FRET imaging was performed at the DZNE Light Microscopy Facility using the Andor Spinning Disk Setup (built on an inverted Eclipse Ti Microscope, Nikon) at 37° C. For FRET imaging, the 445 nm laser (18% intensity, 445-, 514-, 640-triple dichroic mirror in the Yokogawa CSU-X1

unit and 5000 rpm disk speed) was used as excitation source, combined with a dual-cam CFP/YFP filter cube (509 nm dichroic mirror with 475/25 nm and 550/49 nm emission filters) to simultaneously measure cerulean and citrine emission with the two EM-CCD cameras (100 ms exposure time, 300 EM gain, 5.36 frames per second frame rate, 10.0 MHz horizontal readout, 1.7 µs vertical readout time, 5x pre Amp gain, -70° C camera temperature). The imaging procedure was as follows: Cells were washed once with ES buffer and measurements were performed in ES buffer. Cilia were imaged with a 100x/1.45 oil objective with 1 µm step size in 10 s intervals. After a stable baseline was obtained, cells were stimulated by drug addition. Cilia-specific fluorescence values were obtained by analyzing the recordings using CiliaQ as described above in "Confocal microscopy and image analysis". The FRET signal was calculated as a ratio of cerulean/citrine, normalized to the mean baseline value before stimulus addition, and plotted as a change over time.

**ELISA-based cAMP measurements**

Total cAMP levels were determined using a CatchPoint™ assay (Molecular Devices) according to manufacturer's instructions. A detailed description can be found in the SI Appendix.

**Zebrafish as an experimental model**

The animal facilities and maintenance of the zebrafish, *Danio rerio*, were approved by the Norwegian Food Safety Authority (NFSA). Detailed information can be found in the SI Appendix. For experiments the following zebrafish lines were used: nacre *(mitfa-/-)* (Lister et al., 1999), *b-actin:arl13b-gfp* (Borovina et al., 2010), and *Ubi:zebrabow* (Pan et al., 2013) transgenic animals, which express RFP ubiquitously in absence of Cre recombinase.

**mRNA synthesis, injection, immunostaining, and imaging**

The mRNA synthesis, injection, immunostaining, and imaging was performed according to standard protocols. Details are described in the SI Appendix.

**Data availability statement**

The datasets generated during and/or analyzed during the current study are available through the following doi 10.6084/m9.figshare.c.4792248.

**Code availability statement**

The analysis workflow to study cilia length and fluorescence signal with its custom-written ImageJ plug-ins ("CiliaQ") and is available through the following link https://github.com/hansenjn/CiliaQ.

**Acknowledgement**

The project was supported by grants from the Deutsche Forschungsgemeinschaft (DFG): SPP1926: grant MO2192/4-1 (to AM) and grant WA3382/2-1 (to DW), SPP1726: grant WA3382/3-1 (to DW), TRR83/SFB (to DW), FOR2743 (to DW), and under Germany's Excellence Strategy – EXC2151 – 390873048 (to DW and FIS), Emmy Noether (to FIS), the Boehringer Ingelheim Fonds (to JNH), and a Samarbeidsorganet Helse Midt-Norge grant (to NJY). We thank Jens-Henning Krause for technical support, the Core Facility Nanobodies of the University of Bonn, and the Core Research Facility for Light Microscopy (CRFS) of the DZNE (German Center for Degenerative Diseases), and the fish facility support team at the Kavli Institute for Systems Neuroscience.

## Declaration of Interests

The authors declare no competing interests.

## Author contribution

DW, JNH, AM, NJY, DUM, and FIS designed the experiments and wrote the manuscript. WB performed the cloning, JNH, RC, FK, NJY, BS, and CV performed the experiments. DW, AM, and FIS acquired the funding to conduct the experiments.

## Additional Information

Supporting information: Supplementary Material & Methods, Supplementary Figures 1-5, and Supplementary Table 1.

## References

Antal MC, Benardais K, Samama B, Auger C, Schini-Kerth V, Ghandour S, Boehm N (2017) Adenylate Cyclase Type III Is Not a Ubiquitous Marker for All Primary Cilia during Development. *PLoS One* 12: e0170756

Ariotti N, Rae J, Giles N, Martel N, Sierecki E, Gambin Y, Hall TE, Parton RG (2018) Ultrastructural localisation of protein interactions using conditionally stable nanobodies. *PLoS Biol* 16: e2005473

Avasthi P, Marley A, Lin H, Gregori-Puigjane E, Shoichet BK, von Zastrow M, Marshall WF (2012) A chemical screen identifies class a g-protein coupled receptors as regulators of cilia. *ACS Chem Biol* 7: 911-9

Balbach M, Beckert V, Hansen JN, Wachten D (2018) Shedding light on the role of cAMP in mammalian sperm physiology. *Mol Cell Endocrinol* 468: 111-120

Barroso I (2018) ADCY3, neuronal primary cilia and obesity. *Nat Genet* 50: 166-167

Beghein E, Gettemans J (2017) Nanobody Technology: A Versatile Toolkit for Microscopic Imaging, Protein-Protein Interaction Analysis, and Protein Function Exploration. *Front Immunol* 8: 771

Beghein E, Van Audenhove I, Zwaenepoel O, Verhelle A, De Ganck A, Gettemans J (2016) A new survivin tracer tracks, delocalizes and captures endogenous survivin at different subcellular locations and in distinct organelles. *Sci Rep* 6: 31177

Berbari NF, Lewis JS, Bishop GA, Askwith CC, Mykytyn K (2008) Bardet-Biedl syndrome proteins are required for the localization of G protein-coupled receptors to primary cilia. *Proc Natl Acad Sci USA* 105: 4242-6

Besschetnova TY, Kolpakova-Hart E, Guan Y, Zhou J, Olsen BR, Shah JV (2010) Identification of signaling pathways regulating primary cilium length and flow-mediated adaptation. *Curr Biol* 20: 182-7

Bishop GA, Berbari NF, Lewis J, Mykytyn K (2007) Type III adenylyl cyclase localizes to primary cilia throughout the adult mouse brain. *The Journal of Comparative Neurology* 505: 562-71

Borovina A, Superina S, Voskas D, Ciruna B (2010) Vangl2 directs the posterior tilting and asymmetric localization of motile primary cilia. *Nat Cell Biol* 12: 407-12

Breslow DK, Koslover EF, Seydel F, Spakowitz AJ, Nachury MV (2013) An in vitro assay for entry into cilia reveals unique properties of the soluble diffusion barrier. *J Cell Biol* 203: 129-47

Cao H, Chen X, Yang Y, Storm DR (2016) Disruption of type 3 adenylyl cyclase expression in the hypothalamus leads to obesity. *Integr Obes Diabetes* 2: 225-228

Cao M, Meng D, Wang L, Bei S, Snell WJ, Pan J (2013) Activation loop phosphorylation of a protein kinase is a molecular marker of organelle size that dynamically reports flagellar length. *Proc Natl Acad Sci USA* 110: 12337-42

Delling M, DeCaen PG, Doerner JF, Febvay S, Clapham DE (2013) Primary cilia are specialized calcium signalling organelles. *Nature* 504: 311-4

Delling M, Indzhykulian AA, Liu X, Li Y, Xie T, Corey DP, Clapham DE (2016) Primary cilia are not calcium-responsive mechanosensors. *Nature* 531: 656-60

Fridy PC, Li Y, Keegan S, Thompson MK, Nudelman I, Scheid JF, Oeffinger M, Nussenzweig MC, Fenyo D, Chait BT, Rout MP (2014) A robust pipeline for rapid production of versatile nanobody repertoires. *Nat Methods* 11: 1253-60

Gasser C, Taiber S, Yeh CM, Wittig CH, Hegemann P, Ryu S, Wunder F, Moglich A (2014) Engineering of a red-light-activated human cAMP/cGMP-specific phosphodiesterase. *Proceedings of the National Academy of Sciences of the United States of America* 111: 8803-8

Götzke H, Kilisch M, Martinez-Carranza M, Sograte-Idrissi S, Rajavel A, Schlichthaerle T, Engels N, Jungmann R, Stenmark P, Opazo F, Frey S (2019) A rationally designed and highly versatile epitope tag for nanobody-based purification, detection and manipulation of proteins. *BioRxiv*

Grarup N, Moltke I, Andersen MK, Dalby M, Vitting-Seerup K, Kern T, Mahendran Y, Jorsboe E, Larsen CVL, Dahl-Petersen IK, Gilly A, Suveges D, Dedoussis G, Zeggini E, Pedersen O, Andersson R, Bjerregaard P, Jorgensen ME, Albrechtsen A, Hansen T (2018) Loss-of-function variants in ADCY3 increase risk of obesity and type 2 diabetes. *Nat Genet* 50: 172-174

Guadiana SM, Semple-Rowland S, Daroszewski D, Madorsky I, Breunig JJ, Mykytyn K, Sarkisian MR (2013) Arborization of dendrites by developing neocortical neurons is dependent on primary cilia and type 3 adenylyl cyclase. *J Neurosci* 33: 2626-38

Harmansa S, Alborelli I, Bieli D, Caussinus E, Affolter M (2017) A nanobody-based toolset to investigate the role of protein localization and dispersal in Drosophila. *elife* 6

Hendel NL, Thomson M, Marshall WF (2018) Diffusion as a Ruler: Modeling Kinesin Diffusion as a Length Sensor for Intraflagellar Transport. *Biophys J* 114: 663-674

Herce HD, Deng W, Helma J, Leonhardt H, Cardoso MC (2013) Visualization and targeted disruption of protein interactions in living cells. *Nat Commun* 4: 2660

Hsu KS, Chuang JZ, Sung CH (2017) The Biology of Ciliary Dynamics. *Cold Spring Harb Perspect Biol* 9

Hu Z, Liang Y, He W, Pan J (2015) Cilia disassembly with two distinct phases of regulation. *Cell Rep* 10: 1803-10

Ishikawa H, Marshall WF (2017) Testing the time-of-flight model for flagellar length sensing. *Mol Biol Cell* 28: 3447-3456

Jansen V, Alvarez L, Balbach M, Strünker T, Hegemann P, Kaupp UB, Wachten D (2015) Controlling fertilization and cAMP signaling in sperm by optogenetics. *eLife* 4

Jiang JY, Falcone JL, Curci S, Hofer AM (2019) Direct visualization of cAMP signaling in primary cilia reveals up-regulation of ciliary GPCR activity following Hedgehog activation. *Proc Natl Acad Sci USA* 116: 12066-12071

Johnson JL, Leroux MR (2010) cAMP and cGMP signaling: sensory systems with prokaryotic roots adopted by eukaryotic cilia. *Trends Cell Biol* 20: 435-44

Johnstone TB, Agarwal SR, Harvey RD, Ostrom RS (2018) cAMP Signaling Compartmentation: Adenylyl Cyclases as Anchors of Dynamic Signaling Complexes. *Mol Pharmacol* 93: 270-276

Kaupp UB (2010) Olfactory signalling in vertebrates and insects: differences and commonalities. *Nature reviews Neuroscience* 11: 188-200

Kee HL, Dishinger JF, Blasius TL, Liu CJ, Margolis B, Verhey KJ (2012) A size-exclusion permeability barrier and nucleoporins characterize a ciliary pore complex that regulates transport into cilia. *Nat Cell Biol* 14: 431-7

Keeling J, Tsiokas L, Maskey D (2016) Cellular Mechanisms of Ciliary Length Control. *Cells* 5

Kim S, Tsiokas L (2011) Cilia and cell cycle re-entry: more than a coincidence. *Cell Cycle* 10: 2683-90

Kirchhofer A, Helma J, Schmidthals K, Frauer C, Cui S, Karcher A, Pellis M, Muyldermans S, Casas-Delucchi CS, Cardoso MC, Leonhardt H, Hopfner KP, Rothbauer U (2010) Modulation of protein properties in living cells using nanobodies. *Nat Struct Mol Biol* 17: 133-8

Kramer-Zucker AG, Olale F, Haycraft CJ, Yoder BK, Schier AF, Drummond IA (2005) Cilia-driven fluid flow in the zebrafish pronephros, brain and Kupffer's vesicle is required for normal organogenesis. *Development* 132: 1907-21

Kubala MH, Kovtun O, Alexandrov K, Collins BM (2010) Structural and thermodynamic analysis of the GFP:GFP-nanobody complex. *Protein Sci* 19: 2389-401

Kwon RY, Temiyasathit S, Tummala P, Quah CC, Jacobs CR (2010) Primary cilium-dependent mechanosensing is mediated by adenylyl cyclase 6 and cyclic AMP in bone cells. *FASEB J* 24: 2859-68

Liang Y, Zhu X, Wu Q, Pan J (2018) Ciliary Length Sensing Regulates IFT Entry via Changes in FLA8/KIF3B Phosphorylation to Control Ciliary Assembly. *Curr Biol* 28: 2429-2435 e3

Lister JA, Robertson CP, Lepage T, Johnson SL, Raible DW (1999) nacre encodes a zebrafish microphthalmia-related protein that regulates neural-crest-derived pigment cell fate. *Development* 126: 3757-67

Loktev AV, Jackson PK (2013) Neuropeptide Y family receptors traffic via the Bardet-Biedl syndrome pathway to signal in neuronal primary cilia. *Cell Rep* 5: 1316-29

Ludington WB, Ishikawa H, Serebrenik YV, Ritter A, Hernandez-Lopez RA, Gunzenhauser J, Kannegaard E, Marshall WF (2015) A systematic comparison of mathematical models for inherent measurement of ciliary length: how a cell can measure length and volume. *Biophys J* 108: 1361-1379

Luo M, Cao M, Kan Y, Li G, Snell W, Pan J (2011) The phosphorylation state of an aurora-like kinase marks the length of growing flagella in Chlamydomonas. *Curr Biol* 21: 586-91

Meng D, Pan J (2016) A NIMA-related kinase, CNK4, regulates ciliary stability and length. *Mol Biol Cell* 27: 838-47

Mick DU, Rodrigues RB, Leib RD, Adams CM, Chien AS, Gygi SP, Nachury MV (2015) Proteomics of Primary Cilia by Proximity Labeling. *Dev Cell* 35: 497-512

Moore BS, Stepanchick AN, Tewson PH, Hartle CM, Zhang J, Quinn AM, Hughes TE, Mirshahi T (2016) Cilia have high cAMP levels that are inhibited by Sonic Hedgehog-regulated calcium dynamics. *Proceedings of the National Academy of Sciences of the United States of America* 113: 13069-13074

Mukherjee S, Jansen V, Jikeli JF, Hamzeh H, Alvarez L, Dombrowski M, Balbach M, Strünker T, Seifert R, Kaupp UB, Wachten D (2016) A novel biosensor to study cAMP dynamics in cilia and flagella. *eLife* 5

Mukhopadhyay S, Wen X, Ratti N, Loktev A, Rangell L, Scales SJ, Jackson PK (2013) The ciliary G-protein-coupled receptor Gpr161 negatively regulates the Sonic hedgehog pathway via cAMP signaling. *Cell* 152: 210-23

Nachury MV (2018) The molecular machines that traffic signaling receptors into and out of cilia. *Curr Opin Cell Biol* 51: 124-131

Nachury MV, Mick DU (2019) Establishing and regulating the composition of cilia for signal transduction. *Nat Rev Mol Cell Biol* 20: 389-405

Nordman S, Ding B, Ostenson CG, Karvestedt L, Brismar K, Efendic S, Gu HF (2005) Leu7Pro polymorphism in the neuropeptide Y (NPY) gene is associated with impaired glucose tolerance and type 2 diabetes in Swedish men. *Exp Clin Endocrinol Diabetes* 113: 282-7

Ohta Y, Furuta T, Nagai T, Horikawa K (2018) Red fluorescent cAMP indicator with increased affinity and expanded dynamic range. *Sci Rep* 8: 1866

Olstad EW, Ringers C, Hansen JN, Wens A, Brandt C, Wachten D, Yaksi E, Jurisch-Yaksi N (2019) Ciliary Beating Compartmentalizes Cerebrospinal Fluid Flow in the Brain and Regulates Ventricular Development. *Curr Biol* 29: 229-241 e6

Pan J, Snell WJ (2005) Chlamydomonas shortens its flagella by activating axonemal disassembly, stimulating IFT particle trafficking, and blocking anterograde cargo loading. *Dev Cell* 9: 431-8

Pan YA, Freundlich T, Weissman TA, Schoppik D, Wang XC, Zimmerman S, Ciruna B, Sanes JR, Lichtman JW, Schier AF (2013) Zebrabow: multispectral cell labeling for cell tracing and lineage analysis in zebrafish. *Development* 140: 2835-46

Porpora M, Sauchella S, Rinaldi L, Delle Donne R, Sepe M, Torres-Quesada O, Intartaglia D, Garbi C, Insabato L, Santoriello M, Bachmann VA, Synofzik M, Lindner HH, Conte I, Stefan E, Feliciello A (2018) Counterregulation of cAMP-directed kinase activities controls ciliogenesis. *Nat Commun* 9: 1224

Reiter JF, Blacque OE, Leroux MR (2012) The base of the cilium: roles for transition fibres and the transition zone in ciliary formation, maintenance and compartmentalization. *EMBO Rep* 13: 608-18

Rosenbaum JL, Witman GB (2002) Intraflagellar transport. *Nature reviews Molecular cell biology* 3: 813-25

Saeed S, Bonnefond A, Tamanini F, Mirza MU, Manzoor J, Janjua QM, Din SM, Gaitan J, Milochau A, Durand E, Vaillant E, Haseeb A, De Graeve F, Rabearivelo I, Sand O, Queniat G, Boutry R, Schott DA, Ayesha H, Ali M et al. (2018) Loss-of-function mutations in ADCY3 cause monogenic severe obesity. *Nat Genet* 50: 175-179

Siljee JE, Wang Y, Bernard AA, Ersoy BA, Zhang S, Marley A, Von Zastrow M, Reiter JF, Vaisse C (2018) Subcellular localization of MC4R with ADCY3 at neuronal primary cilia underlies a common pathway for genetic predisposition to obesity. *Nat Genet* 50: 180-185

Stabel R, Stüven B, Hansen JN, Körschen HG, Wachten D, Möglich A (2019) Revisiting and Redesigning Light-Activated Cyclic-Mononucleotide Phosphodiesterases. *J Mol Biol* 431: 3029-3045

Steels A, Verhelle A, Zwaenepoel O, Gettemans J (2018) Intracellular displacement of p53 using transactivation domain (p53 TAD) specific nanobodies. *MAbs* 10: 1045-1059

Stierl M, Stumpf P, Udwari D, Gueta R, Hagedorn R, Losi A, Gartner W, Petereit L, Efetova M, Schwarzel M, Oertner TG, Nagel G, Hegemann P (2011) Light modulation of cellular cAMP by a small bacterial photoactivated adenylyl cyclase, bPAC, of the soil bacterium Beggiatoa. *The Journal of biological chemistry* 286: 1181-8

Van Overbeke W, Wongsantichon J, Everaert I, Verhelle A, Zwaenepoel O, Loonchanta A, Burtnick LD, De Ganck A, Hochepied T, Haigh J, Cuvelier C, Derave W, Robinson RC, Gettemans J (2015) An ER-directed gelsolin nanobody targets the first step in amyloid formation in a gelsolin amyloidosis mouse model. *Hum Mol Genet* 24: 2492-507

Wachten S, Schlenstedt J, Gauss R, Baumann A (2006) Molecular identification and functional characterization of an adenylyl cyclase from the honeybee. *J Neurochem* 96: 1580-90

Wang Y, Ren Y, Pan J (2019) Regulation of flagellar assembly and length in Chlamydomonas by LF4, a MAPK-related kinase. *FASEB J* 33: 6431-6441

Wang Z, Li V, Chan GC, Phan T, Nudelman AS, Xia Z, Storm DR (2009) Adult type 3 adenylyl cyclase-deficient mice are obese. *PLoS One* 4: e6979

Wright KJ, Baye LM, Olivier-Mason A, Mukhopadhyay S, Sang L, Kwong M, Wang W, Pretorius PR, Sheffield VC, Sengupta P, Slusarski DC, Jackson PK (2011) An ARL3-UNC119-RP2 GTPase cycle targets myristoylated NPHP3 to the primary cilium. *Genes Dev* 25: 2347-60

## Figures

### Figure 1

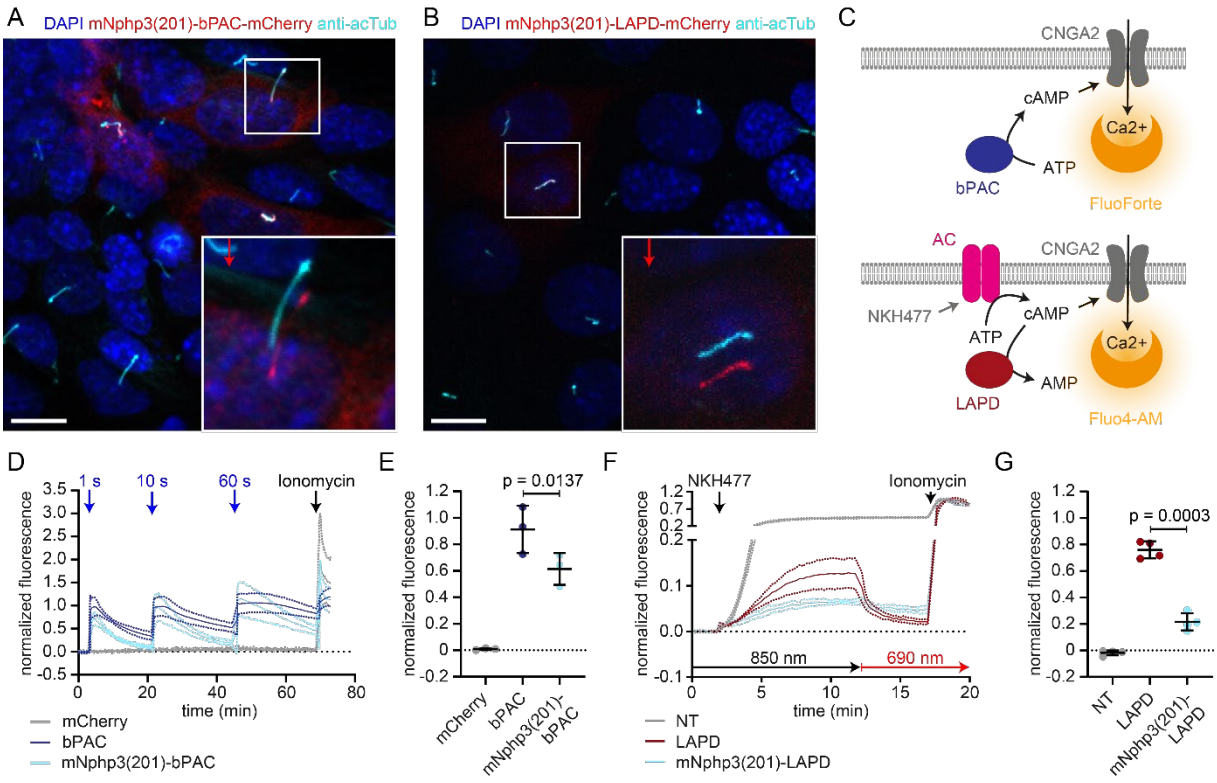


**Figure 1: Direct ciliary targeting of optogenetic tools impairs protein function. A.** Localization of mNphp3(201)-bPAC-mCherry to primary cilia. mIMCD-3 cells expressing mNphp3(201)-bPAC-mCherry were labeled with an anti-acetylated tubulin antibody (cyan, ciliary marker) and with DAPI (blue) to label the DNA. The box indicates the position of the magnified view shown at the bottom right. Red arrow indicates the direction and the length of the shift of the respective fluorescence channel. Scale bar: 10 μm. **B.** Localization of mNphp3(201)-LAPD-mCherry to primary cilia. mIMCD-3 cells expressing mNphp3(201)-LAPD-mCherry were labeled with an anti-acetylated tubulin antibody (cyan, ciliary marker) and DAPI (blue) to label the DNA. The box indicates the position of the magnified view shown at the bottom right. Red arrow indicates the direction and the length of the shift of the respective red channel. Scale bar: 10 μm. **C.** Assays to measure bPAC or LAPD activity using $Ca^{2+}$ imaging. HEK293 cells express the CNGA2-TM ion channel, which opens upon cAMP binding and conducts $Ca^{2+}$ (HEK-TM) (Wachten et al., 2006). Light-dependent activation of bPAC increases intracellular cAMP levels, leading to a $Ca^{2+}$ influx, which was quantified using a fluorescent $Ca^{2+}$ dye (GFP-certified FluoForte). To measure LAPD activity, HEK-TM cells were pre-stimulated with 100 μM NKH477 to activate transmembrane adenylate cyclases (AC), thus increasing cAMP levels. $Ca^{2+}$ influx was detected by a $Ca^{2+}$ dye (Fluo4-AM). **D.** Quantification of bPAC activity. GFP-certified-FluoForte-loaded HEK-TM cells expressing mCherry only (grey), bPAC-mCherry (blue), or mNphp3(201)-bPAC-mCherry (cyan) were stimulated with 465 nm light pulses (1 mW/cm²) of different length and the increase in the intracellular $Ca^{2+}$ concentration was measured. To evoke a maximal $Ca^{2+}$ response, cells were stimulated with 2 μM ionomycin. Data are shown as mean ± SD (dotted lines) for the normalized fluorescence (F-F(baseline))/(F(ionomycin)-F(baseline))/fraction of mCherry-positive cells, n = 3 independent experiments (each data point represents the average of a duplicate or triplicate measurement). **E.** Mean peak amplitudes of the $Ca^{2+}$ signal at 3-6 min after the first light pulse.

Data are shown as individual data points and mean ± SD, n = 3. **F.** Quantification of LAPD activity. Fluo4-AM-loaded HEK-TM cells expressing LAPD-mCherry (red) or mNphp3(201)-bPAC-mCherry (cyan) were incubated with 100 μM NKH477 during continuous 850 nm light stimulation (0.5 μW/cm²). At steady-state, light stimulation was switched to 690 nm (0.5 μW/cm²). NT: non-transfected cells (grey). Data are shown as mean ± SD (dotted lines) for the normalized fluorescence (F-F(baseline))/(F(ionomycin)-F(baseline)). **G.** Mean decrease of the $Ca^{2+}$ signal after 690 nm light stimulation (fraction of maximum value after NKH477 increase), determined over 45 s at 3 min after switching to 690 nm. Data are shown as individual data points and mean ± SD, n = 4 independent experiments (each data point represents the average of a duplicate or triplicate measurement); p-values calculated using a paired, two-tailed t-test are indicated. NT: non-transfected cells.

## Figure 2

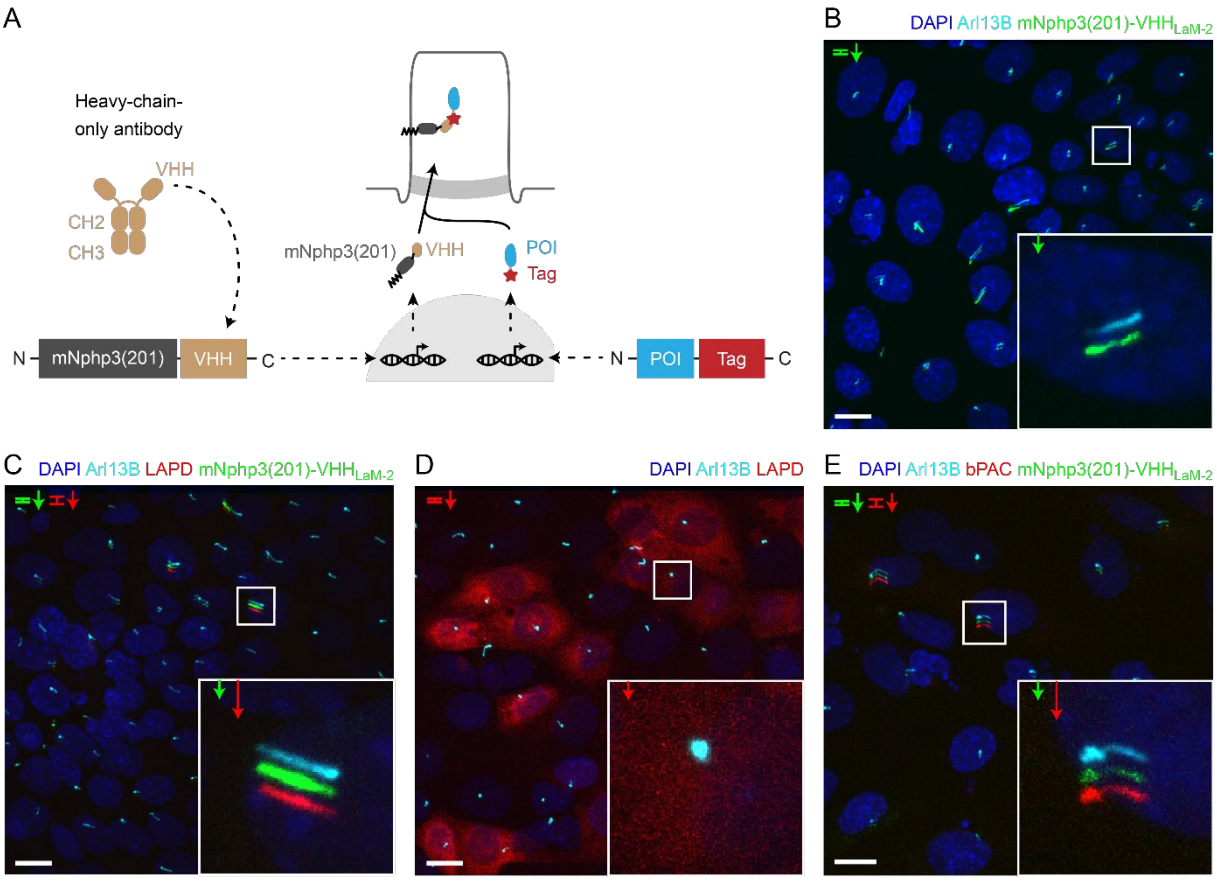


**Figure 2: Targeting optogenetic tools to the primary cilium using nanobodies. A.** Schematic overview targeting approach. Nanobodies were fused to the C terminus of mNphp3(201) for ciliary localization. The protein of interest (POI) is co-expressed with a C-terminal tag or fusion partner that is recognized by the nanobody. Binding of the nanobody to the tag is expected to result in ciliary localization of the POI. **B.** Localization of the anti-mCherry nanobody (VHH$_{LaM-2}$) to primary cilia. mIMCD-3 cells were transfected with mNphp3(201)-VHH$_{LaM-2}$-eGFP (green). **C.** Localization of the anti-mCherry nanobody and LAPD-mCherry to primary cilia. mIMCD-3 cells were co-transfected with mNphp3(201)-VHH$_{LaM-2}$-eGFP (green) and LAPD-mCherry (red). **D.** Cytoplasmic localization of LAPD-mCherry. mIMCD-3 cells were transfected with LAPD-mCherry (red). **E.** Localization of the anti-mCherry nanobody and bPAC-mCherry to primary cilia. mIMCD-3 cells were co-transfected with mNphp3(201)-VHH$_{LaM-2}$-eGFP (green) and bPAC-mCherry (red). All cells shown in B-E were labeled with an Arl13B antibody (cyan, ciliary marker) and DAPI (blue). All scale bars: 10 μm. Boxes indicate the position of the magnified view shown at the bottom right. Arrows in different colors indicate the direction and the length of the shift of the respective fluorescence channel.

**Figure 3**

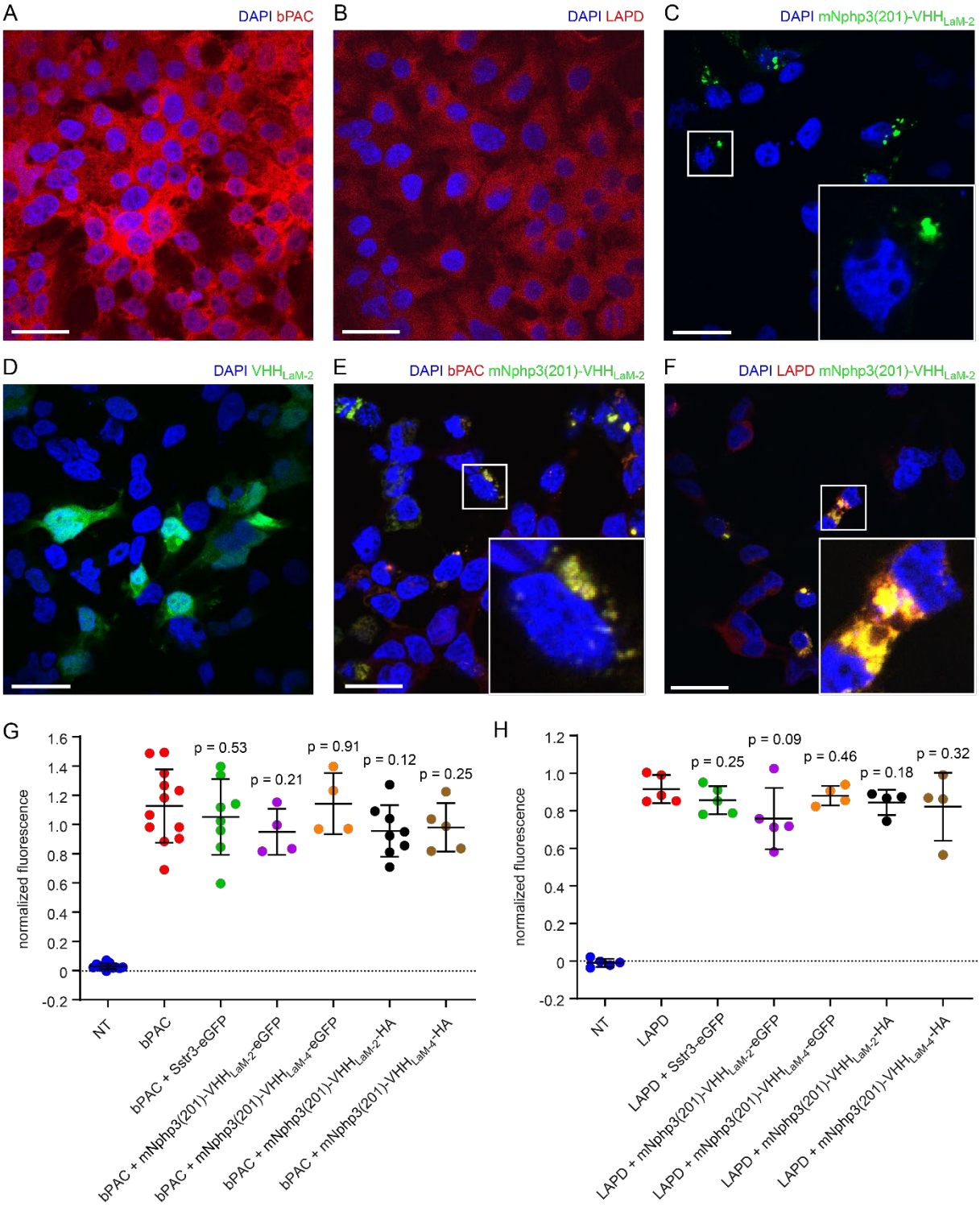


**Figure 3: Functional characterization of nanobody-targeted optogenetic tools. A.** HEK-TM cells expressing bPAC. HEK-TM cells stably expressing bPAC-mCherry (red) were fixed and labeled with DAPI (blue). Scale bar: 20 μm. **B.** See A. for LAPD-mCherry. **C.** HEK-TM cells expressing the cilia-targeted anti-mCherry mNphp3(201)-VHH$_{LaM-2}$-eGFP (green) nanobody. The box indicates the position of the magnified view shown at the bottom right. **D.** HEK-TM cells expressing the cilia-targeted anti-mCherry VHH$_{LaM-2}$-eGFP (green) nanobody. The box indicates the position of the magnified view shown at the bottom right. **E.** Co-expression of the cilia-targeted anti-mCherry nanobody (LaM-2) (green) and bPAC-mCherry

(red) in HEK-TM cells. **F.** Co-expression of the cilia-targeted anti-mCherry nanobody (LaM-2) (green) and LAPD-mCherry (red) in HEK-TM cells. **G.** bPAC activity. bPAC activity was determined in the absence (bPAC) or presence of mNphp3(201)-$VHH_{LaM-2}$ or mNphp3(201)-$VHH_{LaM-4}$ (fused to HA or eGFP). The ciliary protein Sstr3-eGFP was used as a negative control. bPAC activity was determined according to the maximum amplitude of the $Ca^{2+}$ signal after light stimulation (465 nm light pulse, 1 sec, 162 µW/cm²) compared to the ionomycin-evoked $Ca^{2+}$ signal. 5 min before light stimulation, cells were treated with 25 µM of IBMX to inhibit phosphodiesterases and sustain a long-lasting increase in cAMP. NT: non-transfected cells. **H.** LAPD activity. LAPD activity was determined in the absence (LAPD) or presence of mNphp3(201)-$VHH_{LaM-2}$ or mNphp3(201)-$VHH_{LaM-4}$ (fused to HA or eGFP). The ciliary protein Sstr3-eGFP was used as a negative control. Fluo4-AM-loaded HEK-TM cells were incubated with 100 µM NKH477 during continuous 850 nm light illumination (0.5 µW/cm²). When reaching a steady-state, light was switched to 690 nm (0.5 µW/cm²) to stimulate LAPD activity. LAPD activity was determined as the maximal decrease compared to the maximal $Ca^{2+}$ signal amplitude after NKH477 addition. For G and H: NT: non-transfected cells. Data are shown as individual data points (each data point represents and independent experiment and corresponds to the average of a duplicate or triplicate measurement) and mean ± S.D., p-values calculated using unpaired, two-sided Student's t-test compared to bPAC (G) or LAPD (H) only are indicated. All HEK-293 cells were non-ciliated.

## Figure 4

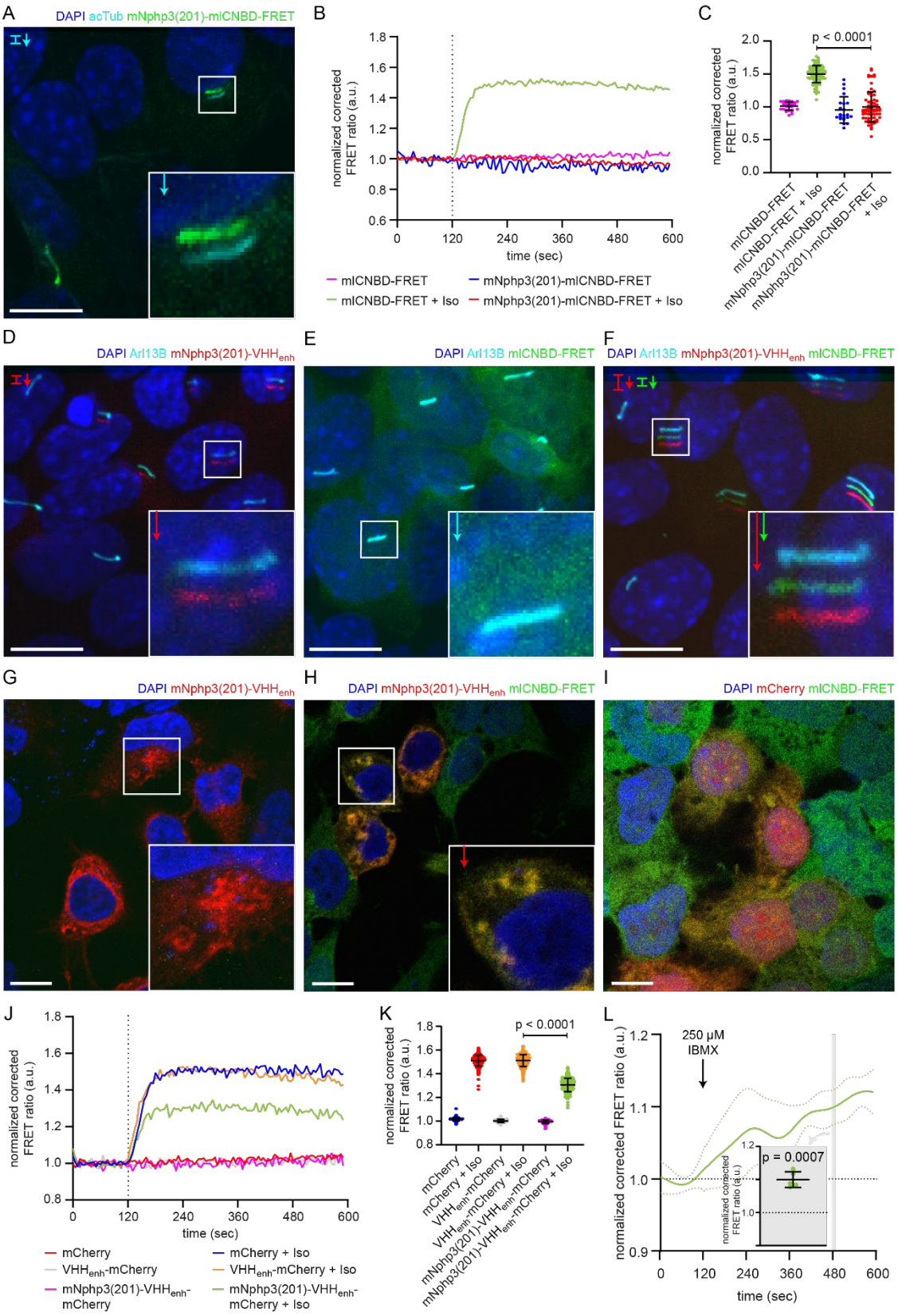


**Figure 4: Functional characterization of nanobody-targeted cAMP biosensor. A.** Localization of mNphp3(201)-mICNBD-FRET to primary cilia in mIMCD-3 cells. **B.** FRET imaging in HEK293 cells expressing mICNBD-FRET or mNphp3(201)-mICNBD-FRET under control conditions or after stimulation with 20 µM isoproterenol (addition depicted with dotted

line). Data are shown as mean (n = 3 independent experiments, 30-90 cells per experiment). **C.** Comparison of the maximal FRET change for data shown in B. Data are presented as individual data points and mean ± S.D.; p-value calculated using an unpaired, two-tailed Mann-Whitney test is indicated. **D**. Localization of the mNphp3(201)-$VHH_{enhancer}$-mcherry anti-eGFP nanobody to primary cilia. **E./F.** Localization of mICNBD-FRET in mIMCD-3 cells in the **E.** absence or **F.** presence of mNPHP3(201)-$VHH_{enhancer}$-mCherry. **G.** Localization of mNphp3(201)-$VHH_{enhancer}$-mCherry in HEK293 cells. **H./I.** Localization of mICNBD-FRET in HEK293 cells in the **H.** presence or **I.** absence of mNphp3(201)-$VHH_{enhancer}$-mCherry. Here, mCherry only was used as a control. **J.** FRET imaging in HEK293 mICNBD-FRET cells transiently co-expressing mCherry, $VHH_{enhancer}$-mCherry, or mNphp3(201)-$VHH_{enhancer}$-mCherry performed under control conditions or after stimulation with 20 μM isoproterenol (Iso, addition depicted with dotted line). Data are shown as mean (n = 3 independent experiments, 30-90 cells per experiment). **K.** Comparison of maximal FRET change for data shown in J. Data are presented as individual data points and mean ± S.D.; p-value calculated using an unpaired, two-tailed Mann-Whitney test is indicated. **L.** FRET imaging in primary cilia of mIMCD-3 cells expressing mICNBD-FRET and mNphp3(201)-$VHH_{enhancer}$-mCherry. Cells have been stimulated with 250 μm IBMX. Data are shown as mean (dark green line) ± S.D. (dotted green line), n = 5. Inset: each data point shows the time-average per cilium at the position indicated by grey box; one-sample Student's t-test compared to 1.0 indicated.

## Figure 5

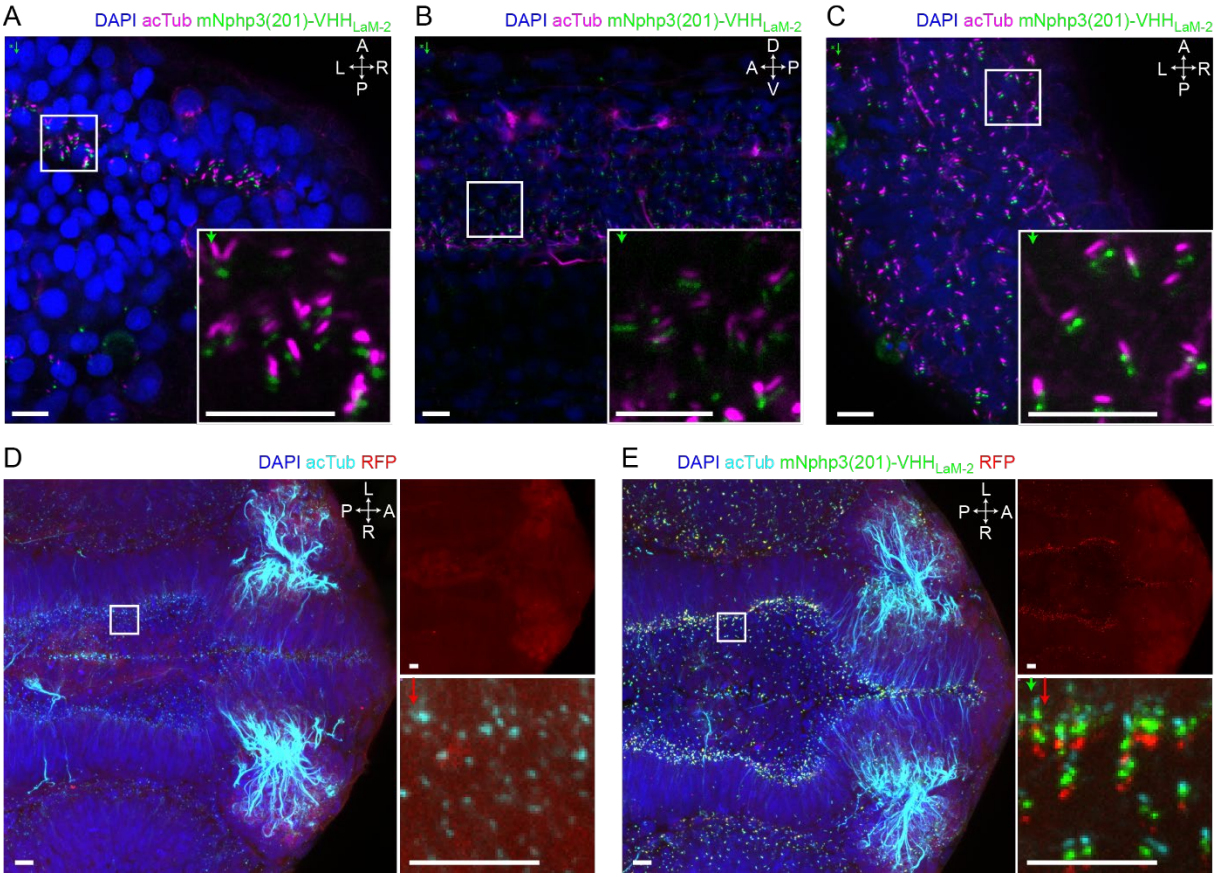


**Figure 5: Nanobody-based ciliary protein targeting *in vivo*. A.** Nanobody localization in the neural tube of a zebrafish embryo. The mRNA of the anti-mCherry mNphp3(201)-VHH$_{LaM-2}$-eGFP nanobody was injected into nacre zebrafish embryos. Embryos were stained with an anti-acetylated tubulin antibody (magenta, ciliary marker), an anti-GFP antibody (green), and DAPI (blue). **B.** see A. for spinal cord. **C.** see A. for eye. **D.** RFP (red) expression in the neural tube of Ubi:zebrabow (Pan et al., 2013) transgenic embryos. **E.** RFP (red) expression in the neural tube of Ubi:zebrabow (Pan et al., 2013) transgenic embryos, injected with mRNA of the anti-mCherry mNphp3(201)-VHH$_{LaM-2}$-eGFP nanobody. Scale bars: 20 μm, magnified view: 10 μm. Boxes indicate the position of the magnified views shown at the bottom right as inset (A-C) or as a separate panel next to the overview image (D, E). Arrows in different colors indicate the direction and the length of the shift of the respective fluorescence channel. The upper right panel in D and E shows the RFP channel only, the bottom right panel shows the magnified view. A: anterior, P: posterior, L: left, R: right, D: dorsal, V: ventral. All images were taken from fixed samples.

## Figure 6

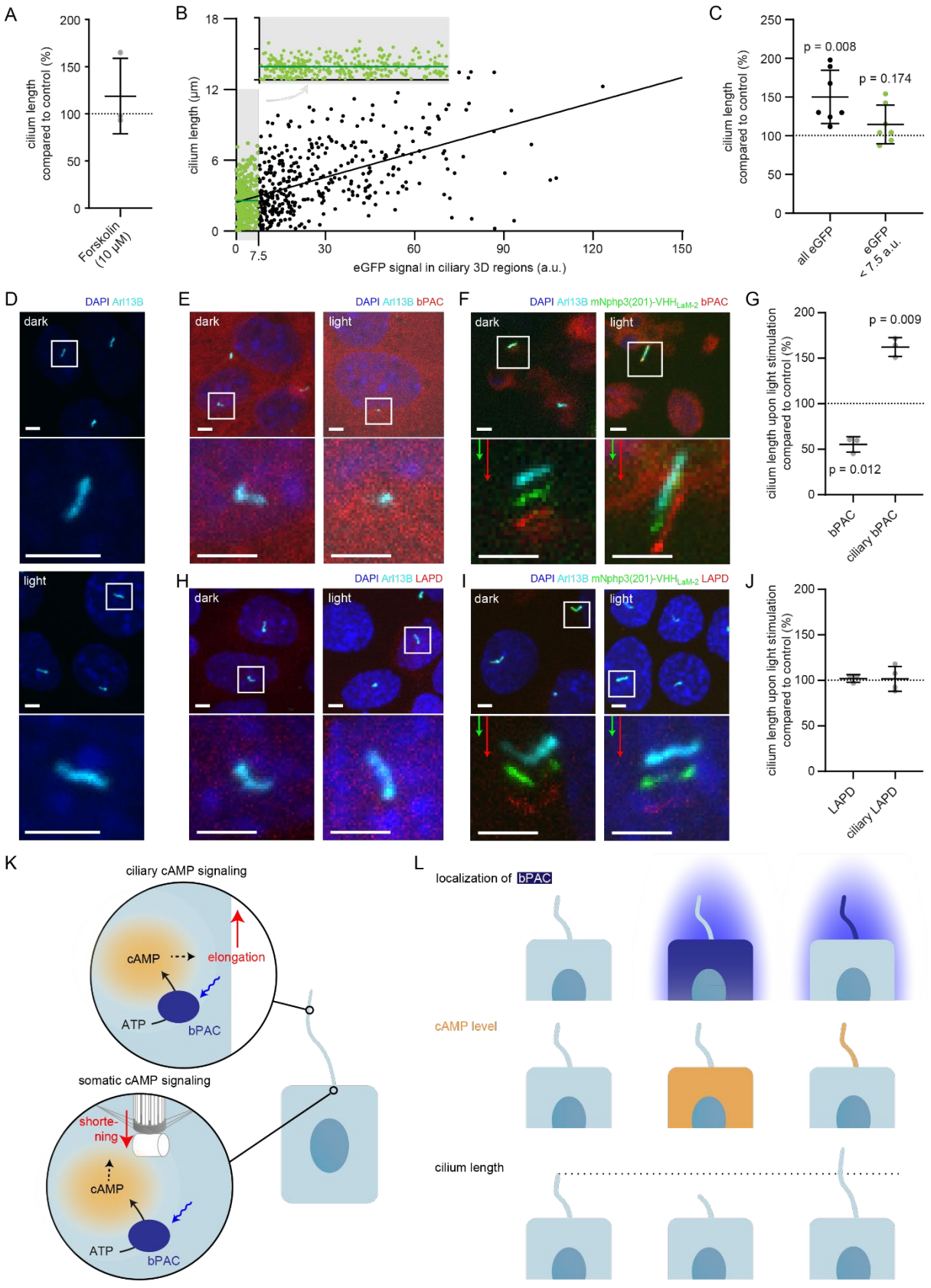


**Figure 6. Controlling cilia length using optogenetics. A.** Cilia length of mIMCD-3 cells stimulated with 10 µM forskolin (solvent: DMSO), normalized to the DMSO control. Data are

shown as mean ± S.D., n = 3 with at least 40 cells per experiment. **B.** Correlation of cilia length and eGFP fluorescence (a.u., average ciliary fluorescence of non-transfected control cells was subtracted) in the cilium in mIMCD-3 cells transiently expressing mNphp3(201)-VHHLaM-2-eGFP. Below 7.5 a.u., the cilia length is independent of the eGFP fluorescence (see inset, values are highlighted in green), whereas including values > 7.5 a.u., there is a linear correlation between the cilia length and the eGFP fluorescence in the cilium. **C.** Length of cilia that show mNphp3(201)-$VHH_{LaM-2}$-eGFP localization and an eGFP fluorescence < 7.5 a.u., normalized to equally treated, non-transfected (NT) control cells. Data are shown as mean ± S.D., n = 7 with at least 18 cilia per experiment; p-values determined using unpaired, two-tailed Student's t-test are indicated. **D.** mIMCD-3 cells (non-transfected, NT) kept in the dark (top) or stimulated with light (bottom, 1 h, 465 nm, 38.8 µW/cm²) **E.** mIMCD-3 bPAC-mCherry cells kept in the dark (left) or stimulated with light (right, 16 h, 465 nm, 38.8 µW/cm²). **F.** mIMCD-3 bPAC-mCherry transiently transfected with mNphp3(201)-$VHH_{LaM-2}$-eGFP kept in the dark (left) or stimulated with light (right, 1 h, 465 nm, 38.8 µW/cm²). **G.** Normalized cilia length after light stimulation (left 1 h, right 16 h; 465 nm, 38.8 µW/cm²) for mIMCD-3 bPAC-mCherry cells with our without transiently expressing mNphp3(201)-$VHH_{LaM-2}$-eGFP. Only cilia with an eGFP fluorescence < 7.5 a.u. were included and each data point was normalized to control cells. Data are shown as mean ± S.D., n = 3 with at least 25 cells per experiment; p-values determined using one-sample Student's t-test compared to 100% are indicated. **H.** mIMCD-3 LAPD-mCherry cells kept in the dark (left) or stimulated with light (right, 16 h, 630 nm, 42.3 µW/cm²). **I.** mIMCD-3 LAPD-mCherry transiently transfected with mNphp3(201)-$VHH_{LaM-2}$-eGFP kept in the dark (left) or stimulated with light (right, 16 h, 630 nm, 42.3 µW/cm²). **J.** Normalized cilia length after light stimulation (16 h, 630 nm, 42.3 µW/cm²) for mIMCD-3 LAPD-mCherry with our without transiently expressing mNphp3(201)-$VHH_{LaM-2}$-eGFP. Only cilia with an eGFP fluorescence < 7.5 a.u. were included and each data point was normalized to control cells. Data are shown as mean ± S.D., n = 3-4 with at least 18 cells per experiment; p-values determined using one-sample Student's t-test compared to 100% are indicated. Cells in D-F and H-I were stained with an Arl13B antibody (cyan) and DAPI (blue). All boxes indicate the magnified view below. Arrows indicate the direction and the length of the shift of the respective same-colored fluorescence channel. Scale bar for all images: 3 µm. **K.** Spatial cAMP signaling controlling cilia length. Our data suggest a model, in which cAMP signaling in the cell body, stimulated by photoactivation of bPAC and an increase in cAMP levels, causes primary cilia shortening, whereas an increase of cAMP levels in the cilium results in primary cilia elongation. **L.** Summary of the correlation between bPAC localization and photoactivation, cAMP levels, and cilia length**.**